FABRICATION AND CHARACTERIZATION OF Al/AlOx/Al JOSEPHSON JUNCTIONS FOR SUPERCONDUCTING QUBITS

By

Reza Firouzmandi

Submitted to graduate school of Engineering and Natural Science

in partial fulfillment of

the requirements for degree of

Master of Science

Sabancı University

Spring 2021

FABRICATION AND CHARACTERIZATION OF Al/AlOx/Al JOSEPHSON JUNCTIONS FOR SUPERCONDUCTING QUBITS

APPROVED BY:

DATE OF APPROVAL: 14/July/2021

© Reza Firouzmandi 2021

All Rights reserved

Abstract

Fabrication and characterization of Al/AlOx/Al Josephson junctions for superconducting qubits

Reza Firouzmandi

Physics, Master of Science Thesis, 2021

Thesis supervisor: Prof. Dr. İsmet İ. Kaya

Keywords: Josephson junction, superconducting qubits, superconductivity, quantum computers

Superconducting circuits are a rapidly evolving field of research for constructing quantum computers and investigating fundamental aspects of quantum mechanics. The primary element of these quantum circuits are Josephson junctions which are supposed to induce non-linearity in the system that is crucial for implementation of quantum two level system(qubit). These qubits or the so-called artificial atoms must satisfy necessary conditions that are called DiVincenzo criteria to be suitable for constructing a quantum computer. The advantage of superconducting circuits is their high scalability potential because of lithographic procedures. However, the fabrication process for Josephson junction is a big challenge because they require optimized process which is not the same in different laboratories because of different machinery configuration and parameters.

In this study, we investigated the fabrication and low temperature characterization of Al/AlOx /Al sub-micron Josephson junctions. We optimized parameters for fabrication of Josephson junctions with equipment available at Sabanci University Nanotechnology Research and Application Center (SUNUM) including spin coating, Electron beam lithography (EBL), resist development, evaporation, aluminum evaporation, and its oxidation. Finally, we represent the characterization result of fabricated junctions.

Özet

Süper iletken kübitler için Al/AlOx/Al Josephson bağlantılarının üretimi ve karakterizasyonu

Reza Firouzmandi

Fizik, Yüksek Lisans Tezi, 2021

Tez danışmanı: Prof. Dr. İsmet İ. kaya

Anahtar Kelimeler: Josephson bağlantısı, süperiletken kübitler, süperiletkenlik, kuantum bilgisayarlar

Süper iletken devreler, kuantum bilgisayarları inşa etmek ve kuantum mekaniğinin temel yönlerini araştırmak için hızla gelişen bir araştırma alanıdır. Bu kuantum devrelerinin birincil unsuru, kuantum iki seviyeli sistemin (kübit) uygulanması için çok önemli olan, sistemde nonlineerite indüklemesi beklenen Josephson bağlantılarıdır. Bu kübitler ya da diğer adıyla yapay atomlar, bir kuantum bilgisayarı inşa etmeye uygun olmaları için DiVincenzo kriterleri olarak adlandırılan gerekli koşulları sağlamalıdır. Süper iletken devrelerin avantajı, litografik prosedürler sayesinde yüksek ölçeklenebilirlik potansiyelleridir. Ancak, Josephson bağlantısı üretim işlemi büyük zorluklar içerir, çünkü farklı laboratuvarlarda farklı enstrümanlar kullanıldığından üretim süreci gereken optimizasyon ve parametreler her laboratuvarda farklı olacaktır.

Bu çalışmada, Al/AlOx/Al alt mikron Josephson bağlantılarının üretimini ve düşük sıcaklık karakterizasyonunu araştırdık. Sabancı Üniversitesi Nanoteknoloji Araştırma ve Uygulama Merkezi'nde (SUNUM) bulunan, spin kaplama, Elektron ışınlı litografi (EBL), direnç geliştirme, buharlaşma, alüminyum buharlaşması ve oksidasyonunu içeren yöntem ve ekipmanlarla Josephson bağlantılarının üretimi için parametreleri optimize ettik ve imal ettiğimiz bağlantıların karakterizasyon sonuçlarını sunuyoruz.

Acknowledgment

First and foremost, I would like to convey my sincere appreciation to Prof. Dr. İsmet İ. Kaya, my advisor. I thank him for all the chances he has given me. Throughout the years, he was more than just an advisor and mentor. It has been an honor for me to learn under his guidance.

I would like to thank the Quantum Transport and Nanoelectronics Laboratory members who helped me during my study with their support and contribution to this project. I wish to express my appreciation to Dr. Vahid Sazgari, Dr. Hadi Khaksaran, Suleyman Celik and Mehmet Kahraman for sharing their knowledge and experience throughout my research and study.

Finally, I would like to express my gratitude to my family for their unwavering support and to all my friends for making my life so enjoyable.

Contents

List of Figures

Introduction

Quantum mechanics has intrinsic properties like superposition and entanglement that has made a revolution in the information theory where it is uncovered that the quantum algorithm processes information exponentially faster than classical computers. This outstanding discovery motivated researchers at the forefront of quantum science to build novel computational processors. However, this so-called quantum computer represents daunting challenges for scientists and engineers. Quantum bits(qubits) are at the heart of quantum computers, and they need to meet exclusive properties. For instance, they are very sensitive to external influence, while classical bits of today's typical computers are not susceptible to such an influence. Over the last two decades, different qubits have been investigated and controlled successfully including qubits originated from spin of electrons or nucleus which have microscopic degrees of freedom, and qubits implemented from macroscopic electrical elements, sometimes can be seen with naked eyes, which are called superconducting qubits. The big challenge in the field is to slow down the decoherence time of the qubits, and at the same time, scaling up the number of the qubits while they are inter-coupled with each other.

Among all the solid-state qubits, superconducting qubits have evolved into a promising platform for future quantum processors and computers. The primary advantage of the superconducting circuits is that they can be scaled up to a larger construction because of nanofabrication techniques. Furthermore, these circuits have macroscopic degrees of freedom because superconductors can be expressed as a single macroscopic wave function[1]; however, this demands that these circuits must be operated at very low temperatures where thermal excitations are suppressed.

The fundamental idea behind the superconducting qubits is to produce nonlinearity in the circuits which creates anharmonicity in the qubit energy levels. This induced anharmonicity separates two of the quantum states from others. Josephson junctions are the best well known source of nonlinearity so far. Josephson junctions are constructed from two layers of superconducting thin films coupled via a very thin layer of insulator barrier. Superconducting qubits, also called Josephson qubits, are divided into two major groups according to the quantum variable that determines their quantum states for the operation of the qubit. In a charge qubit[2], the governing quantum variable is charge, the

presence or absence of excess cooper pairs in a superconducting island defines the two quantum states that process the quantum information. In a flux qubit[3], the quantum variable is flux, two opposite supercurrents circulating around a loop containing three Josephson junctions carry the qubit information and it was experimentally demonstrated one year after the charge qubit. Further engineering of these qubits has led to other types of qubits including quantronium[4], transmon[5], and phase qubit[6].

The fabrication of the superconducting qubit is a big challenge because they need state of the art facilities and optimized nanolithography procedures. Over the years, laboratories around the world have succeeded to improve the fabrication process of superconducting circuits, however it is important to note that parameters and performance factors involved in the fabrication process in any laboratory are different and they need to be optimized. Indeed, this is where the main motivation of this thesis comes from. Our goal at Quantum Transport and Nanoelectronics group (QTNEL) was to achieve a reproducible fabrication procedure for Al/AlOx/Al Josephson junctions that are building blocks of superconducting qubits. During this work, we developed proper procedures and parameters of shadow evaporation technique. In Chapter1, we study the theoretical aspects of Superconductors and Josephson junctions. We briefly describe the historical attempts towards discovery and formulation of superconductivity. Then, we introduce the Josephson junction and the equations governing the nonlinear behavior of it, the rest of the chapter is devoted to brief introduction to superconducting qubits. In Chapter 2, we introduce the experimental techniques required for fabrication of Al/AlOx/Al Josephson Junction including Electron beam lithography (EBL), thermal evaporation, and lift-off. In Chapter3, we discuss the challenges we faced during this work to achieve our objectives. We explain our procedure to fabricate Josephson junction, and cryogenic characterization of the devices.

Finally, we summarize our work during the thesis and give an outlook regarding our future which is fabrication and characterization of superconducting qubits based on the Josephson junctions.

Theory

In this chapter we introduce theoretical aspects of superconducting circuits focusing on Josephson junction which is the aim of this thesis. First, we briefly investigate superconductivity from historical discovery to microscopic explanation of this phenomena.

Then, we describe the essential element in superconducting circuit which is Josephson junction. We introduce two Josephson's equations that describe the behavior of the Junction at superconducting and voltage state. Also, we describe the RCSJ model that is useful to understand some aspects of I-V characteristic of Josephson junction including weak and strong damping.

After learning the essential physics of the Josephson junction, it is time to discuss the applications of this device. We first describe the DC-SQUID, and we explain why DC-SQUID can be used as a magnetometer for extremely small magnetic flux. Finally, we briefly introduce superconducting qubits which are founded on non-linearity of Josephson junction, and at the end of this chapter; flux qubit as an example of superconducting qubit is investigated.

2.1 Superconductivity

It was discovered by Heike Kamerlingh Onnes in 1911 that the resistance of mercury suddenly turns into zero below the critical temperature of the material T_c=4.2K. The next important discovery about superconductors is perfect diamagnetism, which was discovered by Meissner and Ochsenfeld[7] in 1933; and two years later brothers Heinz and Fritz London[8] described the electromagnetic equations of the superconductors:

$$\mathrm{E} = \frac{\partial(\Lambda \mathrm{J}_s)}{\partial t} \tag{1.1}$$

$$\mathrm{B} = -\mathrm{Curl}(\Lambda \mathrm{J}_s) \tag{1.2}$$

$$\Lambda = \frac{m_s}{2e_s^2} \tag{1.3}$$

Where, m_s, e_s and n are defined as mass, charge and density of the particles carrying charge e_s where at the time of formulating it was considered as electron. Eq (1.1) shows that the deviation of the supercurrent over a short period of time which is proportional to

the electric field E and Eq (1.2) shows the expulsion of magnetic field B from superconductor by the induced supercurrent.

Decades later, the microscopic description of superconductors was formulated by Bardeen, Cooper and Schriffer which is known as BCS theory[9]. According to this theory, two electrons with opposite spin and momentum make a pair called "Cooper pair". This happens because of the attractive force between electrons due to exchange of phonons. Since the total spin is zero, they obey Bose-Einstein statistics, and below the critical temperature of the superconductor, all cooper pairs condensed into a lower energy state which is separated by energy Δ from the excited state that includes single electrons.

2.2 Josephson junction

A superconducting device that consists of two separated superconductors coupled via thin barrier which can be insulator or normal metal is called Josephson junction. The focus of this thesis is on the superconductor-insulator-superconductor (SIS) junctions which was predicted and formulated by Brian D. Josephson[10] in 1962. The schematic of Josephson junction and is shown in Figure 2.1

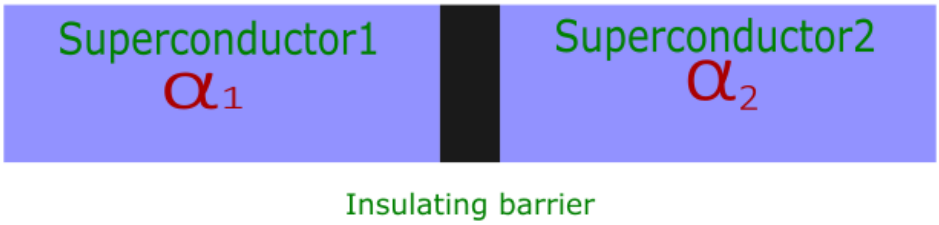

Figure 2.1. Schematic of a Josephson junction. Superconductor 1 with phase α_1 and superconductor 2 with phase α_2 which are separated by a thin insulating barrier.

When the insulating barrier is thin enough, cooper pair can tunnel through the barrier from one superconducting lead to another one. This happens because of the overlap of the macroscopic wave function of the superconducting materials.

2.2.1 Josephson equations

There are two Josephson equations. The first Josephson equation indicates that the supercurrent in the barrier flows without voltage drop and it only depends on the phase difference ($\alpha = \alpha_2 - \alpha_1$) between two superconductors.

$$I = \mathrm{I}_c \sin(\alpha) \tag{1.4}$$

Where I_c is called critical current, which is the maximum current that flows without any dissipation. Below the critical current, there is no voltage drop across the junction and the current only depends on the phase difference α.

The second Josephson equation describes the relation between the voltage across the junction and the evolution of phase difference with respect to time.

$$\frac{\partial(\alpha)}{\partial t} = \frac{2\pi}{\emptyset_0} V \tag{1.5}$$

Where $\emptyset_0 = h/2e = 2.07\text{x}10^{-15}$ Wb is called the magnetic flux quantum, e is the charge of the electron and h is the Planck's constant.

2.2.2 **Josephson energy**

Josephson Junctions have two types of energies that are investigated. The first type is the capacitive energy, and the second one is the coupling energy. Since Josephson junction is consist of two metals separated by thin insulator barrier, it can be considered as a capacitance with area A and a thickness of d and dielectric constant $\mathcal{E}$. Therefore, we can write the capacitive energy E_c:

$$Ec = \frac{e^2}{2C} \tag{1.6}$$

Where $C=\mathcal{E}A/d$ is the capacitance of the junction based on its geometry.

The second energy comes from the binding energy between two superconductors because of the overlap of their wave function. If we write the free energy of the junction based on the two Josephson equations, we can find that:

$$U(\emptyset) = \int_0^t IV dt = \frac{\emptyset_0 I_c}{2\pi}(1 - \cos\alpha) = \mathrm{E}_J(1 - \cos\alpha) \tag{1.7}$$

Where E_J is called Josephson coupling energy.

2.2.3 Current-voltage characteristic

An electrical device can be characterized by its current versus voltage relationship. In the case of Josephson junction, current-voltage characteristic is non-linear as it can be seen in Josephson equations. In a typical I-V curve of Josephson junction Figure 2.2, the voltage across the junction is zero until the current reaches the critical current I_c. This state is called the superconducting state. When the current goes beyond the critical current, it goes into the normal state where it is separated by the superconducting state by a characteristic voltage V_c that depends on the voltage gap (V_g) of the superconducting lead. This voltage gap for the superconductors can be derived as a function energy gap of the material (Δ):

$$V_g = \frac{2\Delta}{e} \tag{1.8}$$

Where V_g is the voltage gap of superconducting metal which is estimated as 360 μV for aluminum[11]. In the normal state, cooper pairs are broken, and single electrons are responsible for conduction. Thus, the Josephson junction becomes a normal conductor with resistance R_n. By sweeping the current back, the voltage goes back to zero at the retrapping current $I_{re} \leq I_c$. Based on the Ambegaokar and Baratoff formula[12], the relationship between critical current I_c and the normal resistance R_n of the junction at low temperature is given by:

$$V_c = I_c R_n = \frac{\pi\Delta}{2e} = \frac{\pi V_g}{4} \tag{1.9}$$

The product of I_cR_n is called characteristic voltage V_c. It can be used to determine the quality of Junctions. For a perfect aluminum Josephson junction, the value of the characteristic voltage is close to 282 μV which can be driven from Eq (1.9).

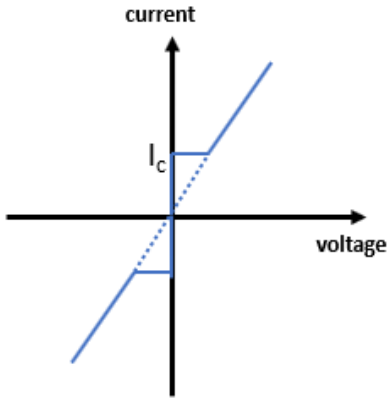

Figure 2.2 I-V characteristic of a Josephson junction. At $|I| \leq I_c$ junction is at superconducting state. At $|I| > I_c$ junction transit to normal state by exceeding the gap voltage V_g.

2.2.4 **RCSJ model**

The dynamics of the Josephson junction can be described by resistively and capacitively shunted junction model (RCSJ model) which was proposed by Stewart and McCumber[13] in 1968. The idea behind this model is to represent the Josephson junction by an equivalent circuit including an ohmic resistor (R_n); and a capacitor (C) shunted with an ideal Josephson junction. Noise sources are ignored for the simplicity.

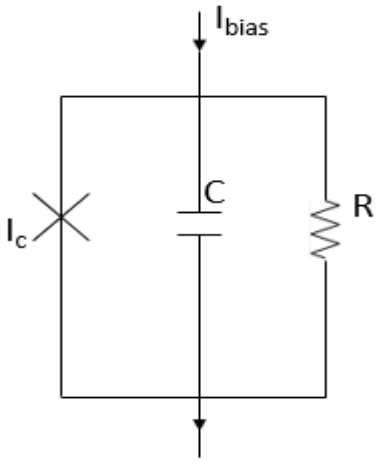

Figure 2.3 circuit diagram of Josephson junction according to RCSJ model.

According to Kirchhoff's law, the total current can be written as sum of the currents flowing through each individual elements:

$$\mathrm{I} = \mathrm{I}_s + \mathrm{I}_n + \mathrm{I}_d = \mathrm{I}_c \sin(\alpha) + \frac{V}{\mathrm{R}_n} + \frac{CdV}{dt} \tag{1.10}$$

Where, $\mathrm{I}_s = \mathrm{I}_c \sin(\alpha)$ is the supercurrent in the non-linear inductor element. $\mathrm{I}_n = \frac{V}{\mathrm{R}_n}$ is the current that flows over the resistor, and $\mathrm{I}_d = \frac{CdV}{dt}$ is the displacement current passing over the capacitor.

Replacing V term using the second Josephson equation in Eq. (1.10) gives:

$$\mathrm{I} = \mathrm{I}_c \sin(\alpha) + \frac{1}{\mathrm{R}_n}\frac{\emptyset_0}{2\pi}\frac{d\alpha}{d\mathrm{t}} + C\frac{\emptyset_0}{2\pi}\frac{d^2\alpha}{dt^2} \tag{1.11}$$

Which is a non-linear differential equation. By substituting the Josephson coupling energy $\mathrm{E}_J = \frac{\emptyset_0 I_c}{2\pi} = \frac{\hbar I_c}{2e}$ into the equation, we obtain

$$\left(\frac{\hbar}{2\mathrm{e}}\right)^2 \mathrm{C}\frac{d^2\alpha}{\mathrm{d}t^2} + \left(\frac{\hbar}{2\mathrm{e}}\right)^2 \frac{1}{\mathrm{R}_n}\frac{\mathrm{d}\alpha}{\mathrm{dt}} + \frac{\mathrm{d}}{\mathrm{d}\alpha}\{\mathrm{E}_J(1 - \cos(\alpha) - \frac{\mathrm{I}}{\mathrm{I}_c}\alpha\} = 0 \tag{1.12}$$

This equation is comparable with the equation of a motion of a particle with mass $m = \mathrm{C}\frac{d^2\alpha}{\mathrm{d}t^2}$ moving in a potential *U(α)*. The quantity (*1/RC*) indicates the damping of the particle, U(α) can be written:

$$\mathrm{U}(\alpha) = E_J\left\{1 - cos(\alpha) - \frac{I}{I_c}\alpha\right\} \tag{1.13}$$

This potential is the so-called washboard potential. In this analogy, the phase α is like a virtual particle. Applying the current bias, tilts the washboard potential (Figure 2.4). If the supercurrent is less than the critical current ($I < I_c$), the phase of the junction does not change which means in the analogy schematic, the particle is trapped in the local potential

well. In results, the voltage development is zero according to Eq (1.5). For $I > I_c$, the current bias tilts the washboard potential so that the phase particle can slip out of the potential well, therefore, voltage develops accordingly. By reducing the current, the washboard potential tilts back again, thus, the phase particles fall into the local trap in the rewrapping current $I_{re} \leq Ic$.

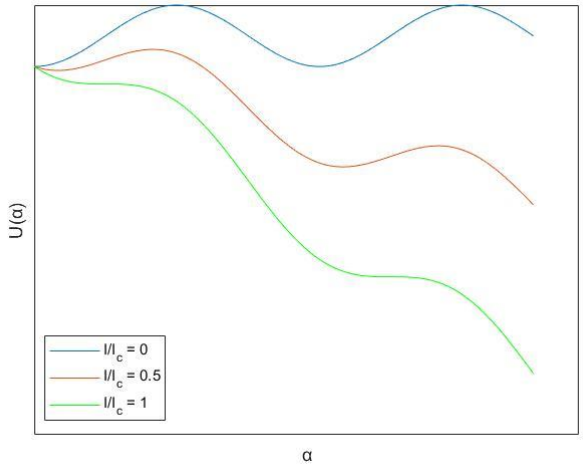

Figure 2.4 Washboard potential plot. Josephson junction is analogous to a moving particle in a washboard potential. Changing the bias current would tilt the potential.

2.2.5 Underdamped and overdamped Junctions

The Stewart and McCumber parameter is introduced to study the mechanism of the retrapping current in a Josephson junction:

$$\beta_c = \frac{2\pi I_c R_n{}^2 C}{\emptyset_0} \tag{1.14}$$

If $\beta_c << 1$, the particle is small, and the damping is large. This means that when the potential is tilted back, the particle can immediately go back to its initial position. In this case there is no hysteresis in the junction, and it is called “overdamped” Junction (Figure 2.5.a).

If $\beta_c >> 1$, the particle is large, and damping is small. If we sweep the current back, the particle will not stop unless the potential is tilted back to the horizontal position. This will result in the hysteretic I-V characterization for the junction (Figure 2.5.b).

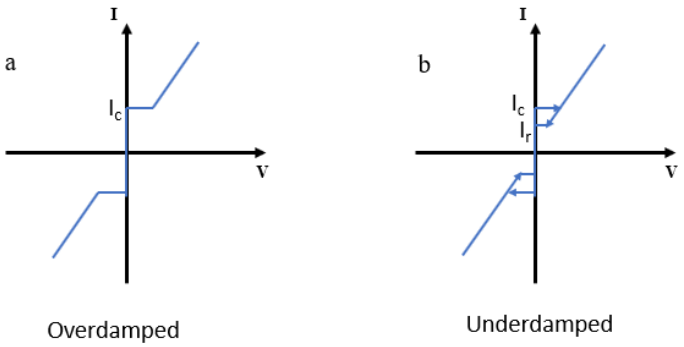

Figure 2.5 The I-V curve of the Josephson junction. a) overdamped junction: the capacitance and resistance are both small. There is no hysteresis in the plot. b) underdamped junction: the capacitance and resistance are large; it takes some effort for the junction to go back to the superconducting state; therefore, there is hysteresis in the I-V characteristic.

Stewart and McCumber parameter can also be determined by the hysteresis in the junction. It is a common way to calculate how damped the junction is.

$$\beta_c = \frac{16}{\pi^2}\left(\frac{I_c}{I_r}\right)^2 \qquad (1.15)$$

Where the I_c is the critical current and I_r is the retrapping current which is the current that needs to be reached so that the junction switches to the superconducting state.

2.3 DC-SQUID

A superconducting loop containing two Josephson junctions in parallel is called D.C. superconducting quantum interference device (DC-SQUID). One of the applications of the DC-SQUID is measuring the magnetic flux entering to this device with high sensitivity up to one quantum flux. In general, DC-SQUID works based on the interference of the phase of the junctions in the loop. To keep it simple we investigate the dc-squid with two identical junctions which means that the junctions have identical critical current I_c.

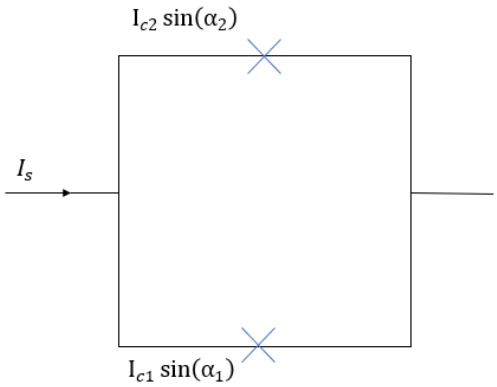

Figure 2.6 Schematic diagram of a DC-SQUID. Superconducting current passes through any of the junction can be written based on the critical current and phase across the junction.

By applying the Kirchhoff's law, the total supercurrent I_s in the loop can be written:

$$I_s = I_{c1}\sin(\alpha_1) + I_{c2}\sin(\alpha_2) = 2I_c cos\left(\frac{\alpha_1 - \alpha_2}{2}\right) sin\left(\frac{\alpha_1 + \alpha_2}{2}\right) \quad (1.16)$$

Since the phase around a superconducting loop is quantized, we find that:

$$\alpha_1 - \alpha_2 = \frac{2\pi\emptyset}{\emptyset_0} \quad (1.17)$$

Plugging this into the Eq (1.16) gives:

$$I_s = 2I_c cos\left(\frac{\pi\emptyset}{\emptyset_0}\right) sin\left(\alpha_2 + \frac{\pi\emptyset}{\emptyset_0}\right) \quad (1.18)$$

We can also calculate the maximum super current I_s^{max} which is dependent on the applied flux in the loop:

$$I_s{}^{max}(\emptyset) = 2I_c cos\left(\frac{\pi\emptyset}{\emptyset_0}\right) \quad (1.19)$$

As shown in the Figure 2.7, switching or maximum supercurrent in the dc-squid modulates with phase difference in the loop which can be altered by the external magnetic flux applied to the device. This is analogous to the double slit experiment where the

constructive and destructive pattern occurs because of the phase difference of the beam. The phase difference in the dc-squid is due to the tuning the magnetic flux penetrating through the device while in the double slit experiment it is due to length difference that the beam travel.

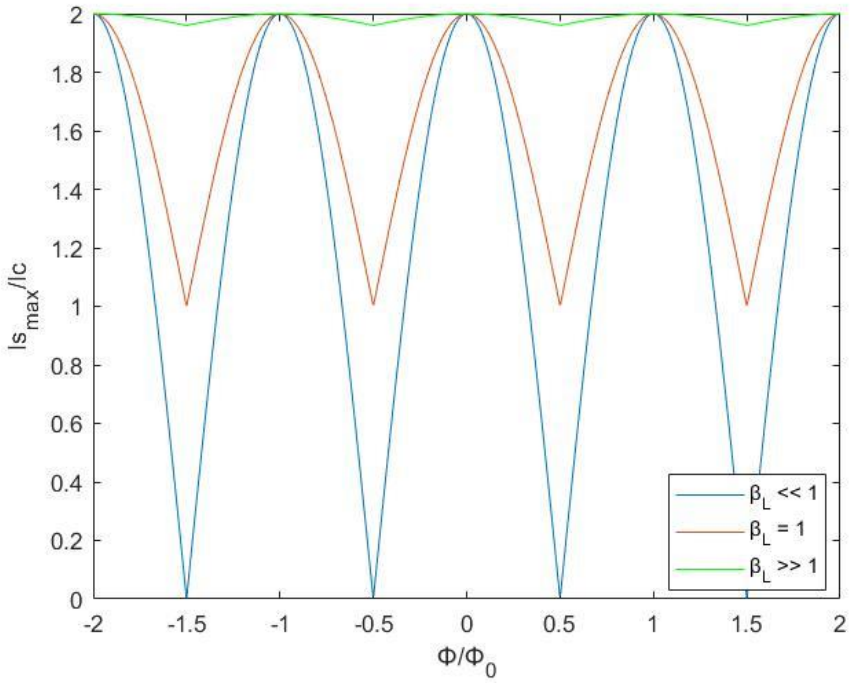

Figure 2.7 Critical current of dc-squid Vs. flux penetrating into the loop for three different screening parameter βL is depicted.

Self-inductance of the dc-squid loop

So far, we have not considered the self-inductance of the dc-squid which also generate some flux penetrating into the loop. Therefore, the real maximum supercurrent in presence of the self-inductance is calculated by considering the real total magnetic flux:

$$\emptyset = \emptyset_{ext} + LI_{cir} \tag{1.20}$$

LI_{cir} is the flux created but the circulating current in the loop; $\emptyset_{ext}$ is the applied external flux and $\emptyset$ is the total flux.

Screening parameter β_L to explain the self-inductance current is written:

$$\beta_L = \frac{2LI_c}{\emptyset_0} \tag{1.21}$$

If $\beta_L << 1$, the flux related to the circulating current is negligible compared to the flux quantum and the external flux, thus, $Ø = Ø_{ext}$. this is the ideal case that we discussed previous sections. (Eq 1.19)

For the case that there is large inductance ($\beta_L >> 1$), the external flux will be compensated to some degree by the circulating current in the loop. Therefore, the maximum supercurrent declines with growing of β_L[14]:

$$\frac{\Delta I_s^{max}(Ø)}{I_c} \approx \frac{1}{\beta_L} \tag{1.22}$$

When the Inductance current is very low, the critical current of the dc-squid modulates between zero and $2I_c$. modulation depth reduces as screening parameter β_L grows up. For $\beta_L = 1$, the maximum supercurrent modulates by half of its value. For $\beta_L >> 1$, In this equation, $\Delta I_s^{max}(Ø)/I_c$ decreases as β_L increases.

2.4 **Superconducting qubits**

Quantum mechanics has introduced new and fascinating concepts such as superpositions and entanglement that yield us to new field of research, and possibilities for quantum technology like quantum computers. In the last two decades, researchers have made enormous effort to develop the hardware for quantum computers that follows certain conditions called DiVincenzo criteria[15]. This hardware relies on the so-called quantum bit(qubit) which is a two-level quantum system. Implementation of qubits has been successful in nuclear magnetic resonance (NMR)[16], ion traps[17], and cavity quantum electrodynamic systems(QED). Although the quantum coherency of these systems is relatively high, they suffer from scalability to a wider structure. In contrast, solid state qubits that are fabricated with state-of-the-art nanolithography techniques have advantage of high scalability, however, because of interaction with multiple degrees of freedom in such systems, they lack in a long quantum coherency time.

Solid state qubits are generally divided in two groups. One is based on the spin of electron, e.g. spin qubit in quantum dot[18]. The other group are based on the Josephson junction and thus superconducting materials. Superconducting qubits are exceptionally promising since the superconducting state has a macroscopic nature which is protected from

environmental dissipation because of the existing superconducting gap, hence, it provides inherent quantum coherency. Josephson junctions, which are the source of non-linearity, play crucial role in superconducting circuits. Over the last two decades, charge qubit[2], flux qubit[3], transmon qubit[5,19],phase qubit[6] , and quantronium[4] has been demonstrated.

Quantum variable in the superconducting qubits is determined by the ratio between flux/phase energy and charging energy. In charge qubit, the coulomb energy is dominant, and the flux/phase energy is smeared out ($E_C/E_J >> 1$), while phase qubit, has small coulomb energy and much larger flux/phase energy ($E_J/E_C >> 1$), three Josephson junction Flux qubit (Sec2.4.3) and transmon qubit stands in intermediate regime where $E_J/E_C \approx 50$. Surprisingly, at this regime, both charge and phase/flux can be utilized as a quantum variable. The transmon qubit is modified version of the charge qubit that succeeded to eliminate the charge noise which is the main drawback of the charge qubits.

2.4.1 Charge and Flux quantization

Superconducting circuits are designed with capacitors, inductors, and Josephson junctions. To formulate the dynamic of the superconducting circuits, it is necessary to apply quantized description. This can be realized by promoting the quantum operators instead of their classical variables:

$$Q \longrightarrow \hat{Q}\ ;\ \emptyset \longrightarrow \hat{\emptyset}$$

Where Q and Ø are representee of the charge and phase/flux. Furthermore, we can write the communication relation of the two conjugate variables as[20]:

$$\left[\hat{\emptyset}, \hat{Q}\right] = -i\hbar \tag{1.23}$$

Where, charge and flux operators can be written down:

$$\hat{Q} = -i\hbar\frac{\partial}{\partial\emptyset}; \hat{\emptyset} = i\hbar\frac{\partial}{\partial Q} \tag{1.24}$$

Also, uncertainty relation can be written:

$$\Delta Q \Delta \emptyset \leq \hbar/2 \tag{1.25}$$

The flux qubit and charge qubit are examples of uncertainty relation. In Sec.2.4.3 we study the flux qubit in more detail.

2.4.2 L-C resonator

Quantum LC-resonator is a quantum electrical circuit containing a capacitor (C), and an inductor (L) coupled in a zero-resistance loop (Figure 2.8). The Hamiltonian of the LC-resonator can be derived following the discussion in Sec.2.4.1.

$$\hat{H}_{LC} = \frac{\hat{\emptyset}^2}{2L} + \frac{\hat{Q}^2}{2C} \tag{1.26}$$

From the quantum mechanics, we know that the Hamiltonian of the simple harmonic oscillator can be written:

$$\hat{H}_{SHO} = \frac{\hat{P}^2}{2m} + \frac{m\omega^2}{2}\hat{X}^2 \tag{1.27}$$

By comparing the Eq (1.26), and Eq (1.27); we find quantities such that, $X \longrightarrow Q$, $P \longrightarrow Q$, and $m \longrightarrow L$. Therefore, the Hamiltonian of the LC-resonator can be derived by creation and annihilation operators:

$$\hat{H}_{LC} = \hbar\omega_{LC}\left(\hat{a}\hat{a}^{\dagger} + \frac{1}{2}\right) \tag{1.28}$$

Where $\omega = 1/LC$, $\hat{a} = \frac{\omega_{LC} L\hat{Q} + i\hat{\emptyset}}{\sqrt{2\hbar\omega_{LC} L}}$,and $\hat{a}^{\dagger} = \frac{\omega_{LC} L\hat{Q} - i\hat{\emptyset}}{\sqrt{2\hbar\omega_{LC} L}}$; also, the creation and annihilation operators obey $[\hat{a}, \hat{a}^{\dagger}] = 1$.

To see the quantum phenomena in this circuits, it should be cooled down to lower temperature such that $k_B T << \hbar\omega$. However, it is not suitable circuit for quantum computing application, because in that case we need a system with only two separated quantum states. This can be realized by adding non-linearity to the system. The source of this non-linearity is the Josephson junction that we covered it in sec. 2.4.2.

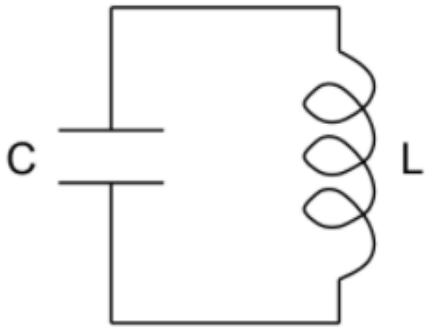

Figure 2.8 Schematic of LC resonator

2.4.3 **Flux qubit**

Flux qubit is a superconducting loop containing one or three Josephson junctions. The former is called RF-squid which we do not cover it in this thesis. Both have same basic principle; however, the flux qubit consists of three Josephson junctions has more reputation and application among scientists because of practical reasons. The size of the junctions is small in flux qubit so that Josephson energy dominates the charging energy by order of E_J/E_C=50; therefore, the quantum variable in this qubit is the flux penetrating into the loop. The two quantum states in qubits are opposite oriented magnetic flux penetrating into the loop or, equivalently, clockwise, and anti-clockwise current flowing in the device. Figure 2.9 shows schematic of flux qubit and a dc-squid around it. The dc-squid is for the readout of the qubit. Two junctions in the qubit are identical while the third one is smaller by factor $0.5 < \gamma < 1$.

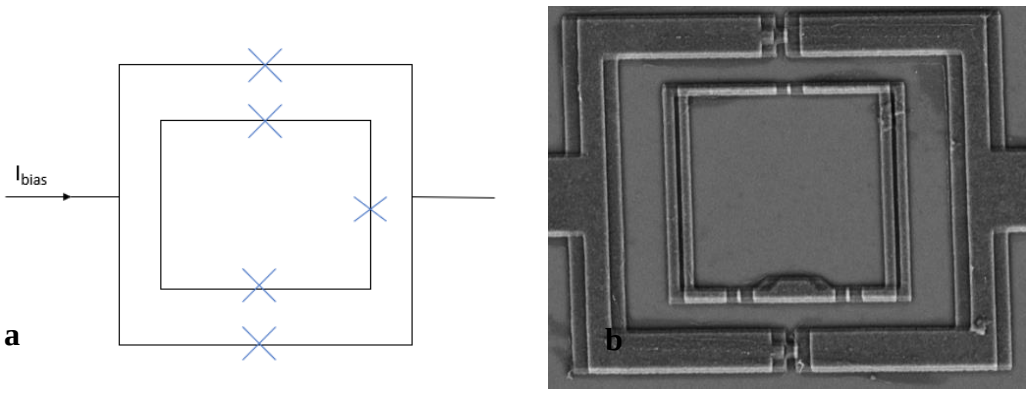

Figure 2.9 Flux qubit. a) Schematic of three Josephson junction flux qubit. b) scanning electron micrograph (SEM) of flux qubit and a DC-SQUID fabricated during this work. DC-SQUID is served for readout of the quantum states.

We determine the qubit potential energy from Josephson energy Eq (1.7), which is sum of three single Josephson junction energy:

$$U(\alpha_1, \alpha_2, \alpha_3) = E_J[(1 - cos\alpha_1) + (1 - cos\alpha_2) + \gamma(1 - cos\alpha_3)] \quad (1.29)$$

Again by using the flux quantization rule in a loop, we can eliminate the smaller junction phase α_3:

$$\alpha_1 - \alpha_2 + \alpha_3 = -2\pi\frac{\emptyset_{ext}}{\emptyset_0} \quad (1.30)$$

Also, by modifying the phase coordinates $\alpha_+ \equiv (\alpha_1+\alpha_2)/2$ and $\alpha_- \equiv (\alpha_1-\alpha_2)/2$, we derive the potential of the qubit:

$$U(\alpha_+, \alpha_-) = E_J\left[2 + \gamma - 2cos\alpha_+ cos\alpha_- - \gamma cos\left(2\pi\frac{\emptyset_{ext}}{\emptyset_0} + 2\alpha_-\right)\right] \quad (1.31)$$

This equation illustrates periodic double-well potential for $\gamma>0.5$. At $\emptyset_{ext} = (n+1/2)$, where n is an integer, the equation turns into symmetrical double well potential. For this degeneracy point, the variation of the ground state and excited state of the qubit is Δ. Apart from the degeneracy point, the energy difference is:

$$\nu = E_e - E_g = \sqrt{\varepsilon^2 + \Delta^2} \quad (1.32)$$

Where $\varepsilon = 2I_q(\emptyset_{ext}-\emptyset_0)$, I_q is the persistent current flowing in the qubit. The probability of observing either of the two quantum states is ½.

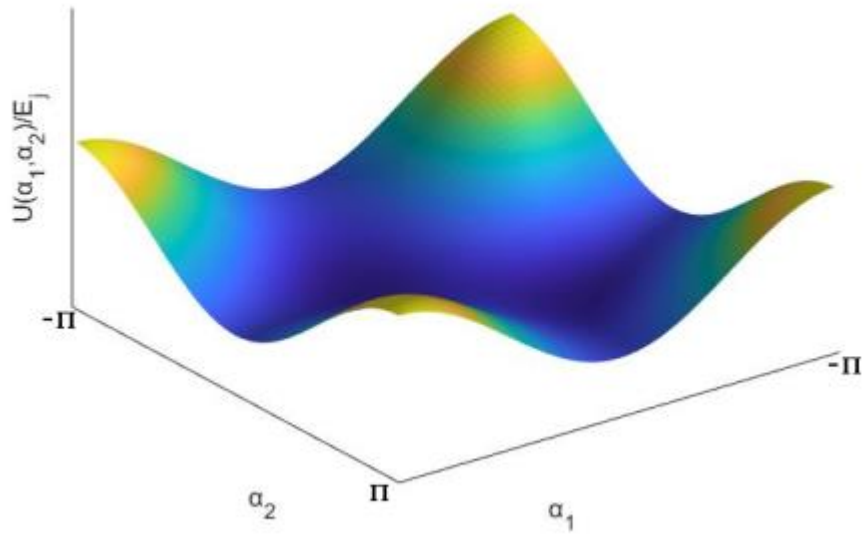

Figure 2.10 The potential diagram for 3-Josephson junction flux qubit for γ=0.8 and $Ø_{ext}/Ø=\frac{1}{2}$. Two potential wells are indication of the persistent current in opposite direction.

Experimental Techniques

In this chapter we introduce the experimental considerations for fabrication of Josephson Junction based on the shadow evaporation technique. The fabrication process depends on the state of art facilities like cleanroom environment, and the aim of this work is to optimize a reliable process based on the equipment at the Sabanci University Nanotechnology Research and Application Center (SUNUM).

Since the Josephson junction fabrication in this thesis are sub-micron dimensions, Electron beam lithography (EBL) system is a compulsory. We first, introduce spin coating process which is an essential part for preparing the samples for EBL process. After Introducing EBL, shadow evaporation technique is explained. Next, we show our homemade thermal evaporation system and finally lift-off process is demonstrated.

3.1 Spin coating

Spin coating is a technique widely used in industry and research facilities for fabrication of nano/microstructure. The biggest advantage of spin coating technique is producing uniform and homogeneous thin layer of resist easily and quickly. There are few stages for spin coating process, first the substrate to be coated is placed on the stage inside the spin coater, then some amount of liquid resist is cast on the substrate with a pipette, and substrate is spun to a determined speed (typically > 600rpm). During the spinning of the substrate, because of the centrifugal force, the solution spreads radially to the edge of the substrate. While the liquid resist become thinner, the viscosity of the resist increases because of the evaporation of the solvent. As a result, solid layer of film forms[21].

Speed of spinning the substrate is one of the most critical factors in spin coating process. The spin speed determines the degree of radial force inserted to the liquid resist and also it effects the velocity and characteristic turbulence of the air immediately above it[22]. The final thickness of the resist is generally determined by the high spin speed. The resist thickness is a result of the interaction between force that drag the resist toward the edge of the sample and the drying rate that impact the viscosity of the fluid. At the point that the fluid is dried, the increasing of the spinning time will not change the resist thickness.

Figure 3.1Phtograph of spin coater at SUNUM

3.2 Electron Beam Lithography (EBL)

Electron Beam Lithography (EBL) is a common fabrication technique used to produce nanostructure. They are preferable for small features comparing with the optical lithography because of the shorter wavelength of the electrons than the light. To write the desired pattern, the sample is deposited with thin layer of resist. When the sample is exposed to the electrons by EBL, the chemical properties of the resist changes and becomes soluble in "developer" which is a specific solution to eliminate the exposed area.

Polymethyl-methacrylate (PMMA) is a common E-beam resist used for making the patterns on the substrate. One of the factors that determines the resolution of the EBL process is the molecular weight of the PMMA. When the molecular weight increases, the PMMA become less sensitive to the electrons, as a result, the development rate decreases which means they have a better resolution comparing with the PMMA with low molecular weight. For the Josephson junction fabrication, two layers of resist with different molecular weight is needed because the undercut in the bottom layer is crucial for the junction overlap. PMMA is coated on the substrate by spin coating process. After spin coating, the samples are baked on the hot plate or in an oven for certain temperature and time to make sure that the reaming solvent is disposed.

When spin coating process is completed, the sample is ready for exposure by EBL. Basically, EBL is developed from scanning electron microscope (SEM). Both systems are equipped with an electron source (gun) and a column in which the electrons are

accelerated and focused by array of electromagnetic lenses. For different applications, it is possible to determine the current value, energy of the beam, and beam diameter. In case of the EBL, there is a moving stage that can raster meticulously the sample and expose the desired area.

When writing the pattern with EBL is done, the sample are inserted into specific chemicals to dissolve the expected regions. MIBK is a common chemical for developing PMMA, but it has very high developing rate. Thus, mixture of IPA and MIBK is typically used for development process to slower than the development duration.

The development process, and EBL dose are two pivotal factors for fabrication of reliable Josephson junctions with shadow evaporation technique because they determine the undercut that produces in the resist profile. If the undercut is not large enough, the evaporated Al at two different angles may not cross each other and overlap of the junction does not happen.

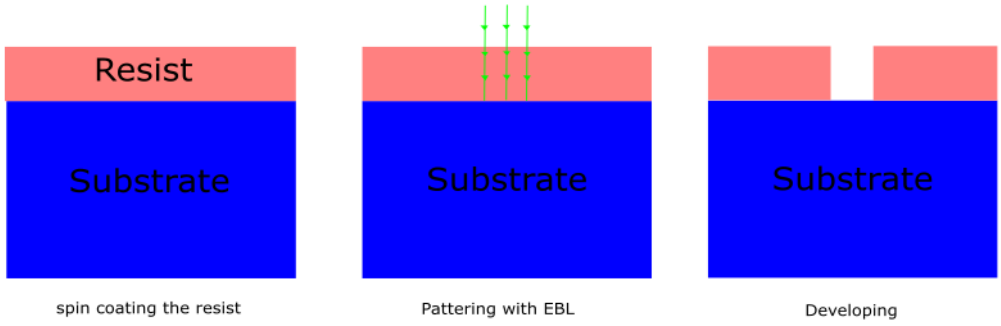

Figure 3.2 Schematic of the EBL process

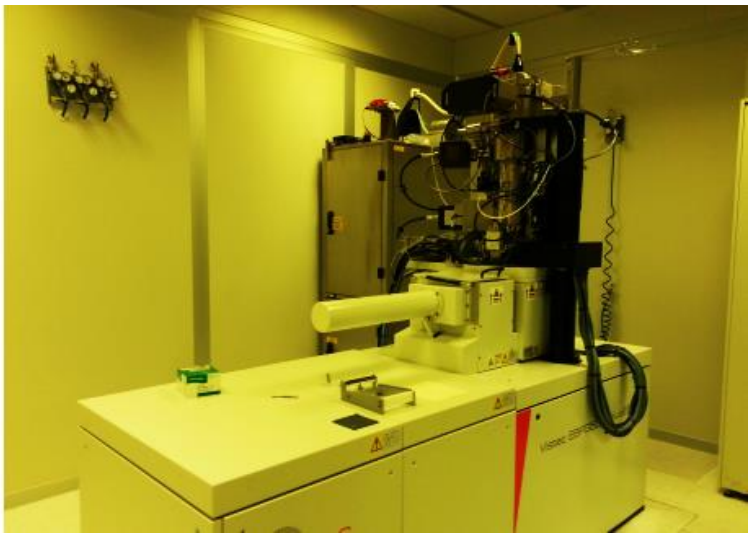

Figure 3.3 Vistec EBPG5000+ES 100 kV electron beam lithography system at SUNUM.

3.3 Shadow evaporation technique

Shadow evaporation also called Dolan technique[23] is a conventional technique that is used to fabricate sub-micron Al/AlO_x/Al Josephson junctions. This method uses a suspended bridge on top of the substrate which can be realized by using two layers of resist. The first layer is a supportive layer that determines the undercut which is a thicker resist, and the second layer or the top layer serves to make a shadow pattern due to the suspended bridge. After patterning the devices by EBL and development of the resist, the samples are ready for evaporation. Figure 3.4 illustrates the process.

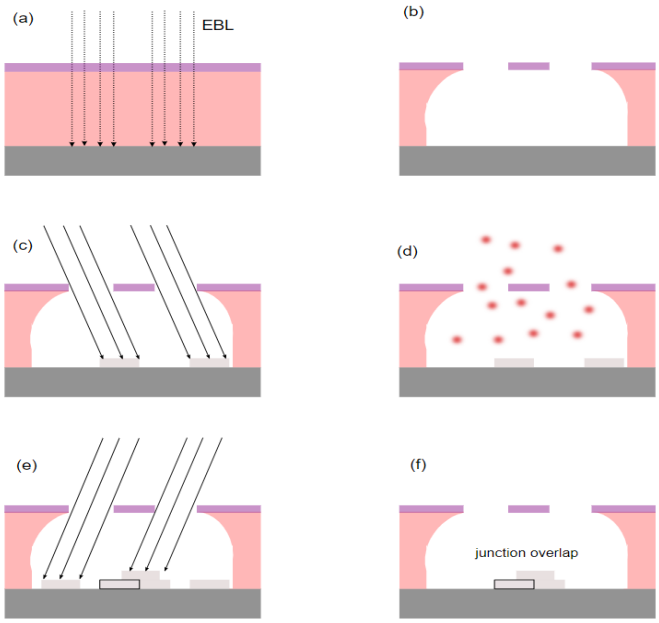

Figure 3.4 Schematic of the shadow evaporation technique a) patterning on double layer resist with EBL, b) development, c) first layer evaporation, d) in-situ oxidation, e) second layer evaporation, f) lift-off; schematic is inspired from reference[24].

After evaporation of the first layer of aluminum at a certain angle, oxygen is purged into the chamber to oxidize the first layer. Oxidation must be in a controlled manner such that a thin layer of aluminum oxide creates. Then, second layer of aluminum is evaporated from another angle to perform an overlap. This overlap of the aluminum and a thin layer of oxide in between is the Al/AlO_x/Al Josephson junction. Finally, the remaining resist is dissolved in acetone and lifts off the undesired aluminum.

3.4 **Josephson junction overlap**

The area that two layers of the evaporated Al overlap with each other has an important role for the fabrication process because it defines the junction properties. In the future of our work, we need Josephson junctions for superconducting qubits, thus making junctions with identical overlap area is crucial. The overlap dimension depends on the thickness of bottom resist (D), the angle that metal is evaporated (θ), and the opening area on top layer (W) which is determined by the layout design of the junctions. However, this calculation is not always precise because the spin coating process does not yield to purely homogeneous resist. SEM images of the samples can be a good way to analyze the dimensions of junction.

The length of the junction overlap(L) can be calculated from Figure 3.5as following:

$$L = \mathrm{D}.\tan(\theta) + \mathrm{D}.\tan(\theta) - W = 2\mathrm{D}.\tan(\theta) - W \qquad (2.1)$$

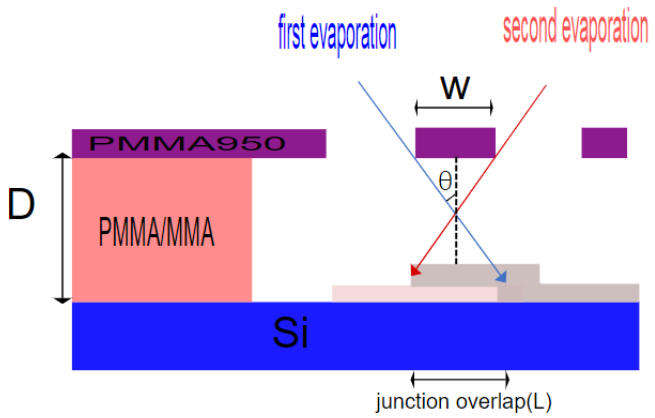

Figure 3.5 Geometric schematic of the Josephson junction overlap.

3.5 Thermal evaporation

Evaporation and oxidation highly affect the quality of the junctions, and one of the purposes of this thesis is to obtain a controlled procedure for them. The metal that we use for fabrication of the Josephson junctions during this work is aluminum which has melting point of 660°C. The evaporation rate is an important factor that determines the roughness of the coated aluminum.

Thermal evaporation takes place in vacuum by heating resistive source like a boat or basket by applying current to evaporate material to form a thin film. When the sufficient vapor pressure is produced, the material starts coating. High vacuum condition is essential for the process because of two reasons[25]: first is that the provided vacuum prevent the vapor to collide with other gas molecules inside the chamber. Otherwise, vapors change their direction during traveling to the sample which leads to poor coverage of the sample. seconds, high vacuum provides a pure deposition. Background gasses in the chamber can generate impurity of the deposited metal. For the case of Josephson junctions, it is very crucial because evaporating the Al in presents of air or oxygen molecules in the chamber results in aluminum oxide instead of pure aluminum film.

We performed the evaporation and oxidation process with a homemade high vacuum thermal evaporation system (Figure 3.6). The system consists of three sources that can be used for different material which are heated by a DC- power supply. It takes few hours for the system to reach 10^{-7} mbar with the help of the turbo pump and a scroll pump. The pressure is monitored by an ion gauge. Furthermore, the stage of the sample holder can rotate using a vacuum step motor in both clockwise and anti-clockwise direction.

The thickness and rate of the deposition is monitored by a quartz crystal inside the chamber. The resonance frequency of the quartz crystal changes when extra mass is deposited on it. The final thickness and deposition rate is calculated by the variation of the resonance frequency of the quartz crystal. Also, a water-cooling system is utilized in the chamber for cooling down the quartz crystal and thus diminishing the thermal fluctuation during evaporation process.

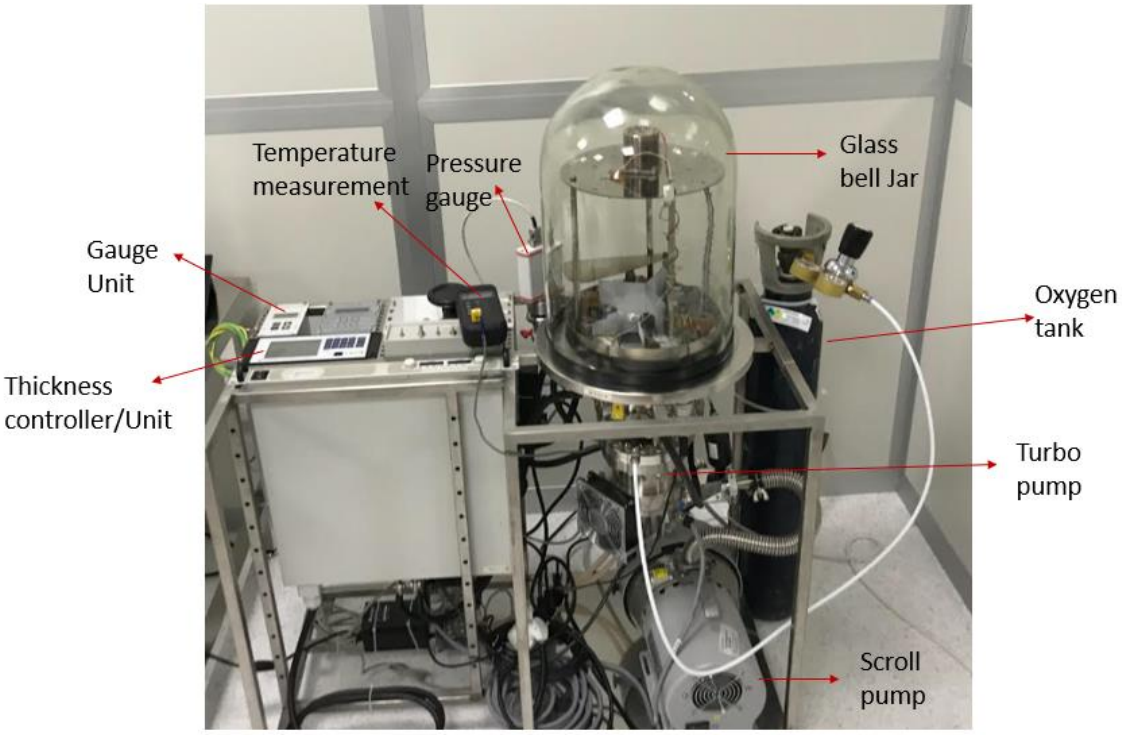

Figure 3.6 Homemade evaporation system (Bell jar) used for fabrication process during this work.

3.6 Lift off

After finishing the evaporation, the extra metal is removed by lift off process. This process is simply working with leaving the samples in proper chemical for certain amount of time. When the sample is immersed into that, any metal stuck to the resist is lifted off and only the metal pattern adherent to the substrate survives.

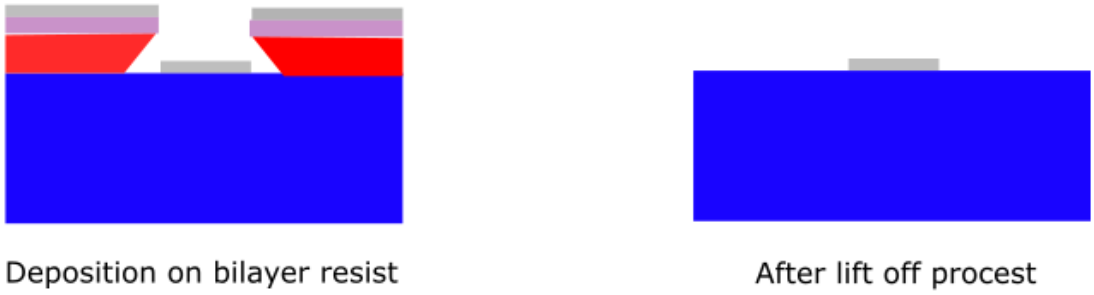

Figure 3.7 Schematic of lift off process

Device fabrication and results

The main goal of this thesis is to optimize and develop a reliable recipe for fabrication of Josephson junctions for superconducting qubits. This chapter contains the process that we have done to achieve this goal. Section 4.1 is about the steps that we found the appropriate double resist system for the shadow evaporation technique. Section 4.2 is dealing with the dose test and for the EBL process and finding a suitable development process. Section 4.3 is devoted to cryogenic characterization of the device and the challenges that we faced.

4.1 Sample preparation

We need to prepare samples ready before doing e-beam lithography. The first step is to clean the Si wafers that are diced into 10x8 mm^2 with diamond scriber. We used acetone and isopropanol (IPA) and ultrasonic bath to clean the samples perfectly, otherwise residue and dirt on the substrate affects the spin coating and thus the electron beam lithography process.

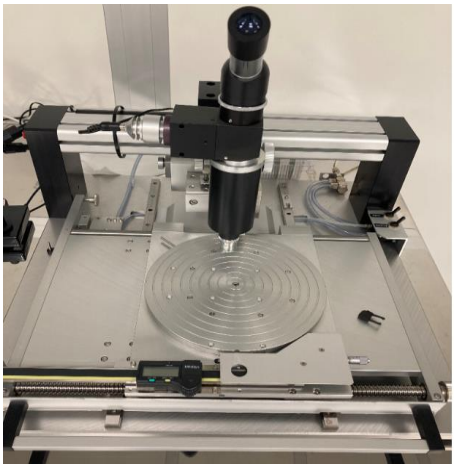

Figure 4.1Photograph of diamond scriber.

4.2 Resist consideration and EBL

According to our evaporation system geometry, the evaporations can be done at angle 15°. This angle requires a certain thickness for the resist that we use. We selected PMMA/MMA EL11 as a bottom layer which gives a thickness of 700 nm at spinning

speed 2500 rpm. For top layer of the resist, we selected PMMA 950 A5 which generates 150 nm thickness at spinning speed 3500 rpm.

Spin speed and spin time determines the thickness of the resist. At the edge of the substrate the thickness is higher because when substrate is spinning the fluid resist starts to evaporate while moving outward, as a result the viscosity of the resist changes according to the radial distance and ends up in a different thickness at the edge. So, we should be careful to leave the edge area empty of sample for EBL patterning. The double layer spin coating process is as follows:

1. Spin coat PMMA/MMA EL11 at 2500 rpm for 60 seconds to generate layer 700nm.
2. Bake the sample at 180 °C for 5 minutes.
3. Spin coat PMMA 950k A5 at 3500 rpm for 60 seconds to generate layer 150nm.
4. Bake the sample at 180 °C for 10 minutes.
5. Blow the sample with nitrogen.

4.2.1 **Dose Test**

The dose to make the pattern with EBL system has an important role in fabrication of Josephson junctions because it affects the size of the undercut. Furthermore, the EBL process determines whether the suspended bridge is produced. To investigate the quality of the undercut and possibility of performing suspended bridges on the bilayer resist, we did dose test with Electron beam lithography on the silicon wafer coated with PMMA/MMA EL11 and PMMA 950 A5. The dose of the electron beam is ranges from 500 to 1300$\mu C/cm^2$ in steps of 25 $\mu C/cm^2$ for this experiment. The sample is coated with thin layer of Al to prevent charging effect during SEM. According to the optical images of the sample (Figure 4.3), suspended bridges forms at higher dose (>700 $\mu C/cm^2$), but they tore up and collapse on the substrate because of the long length of the patterns.

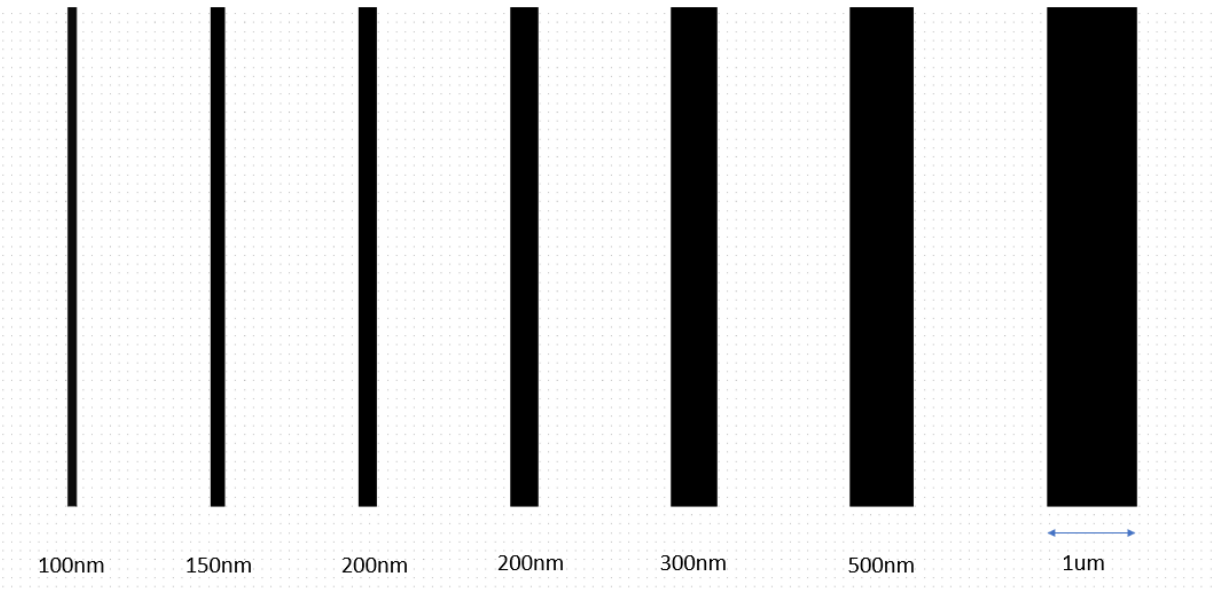

Figure 4.2 The layout design of the parallel lines. The width of the pattern varies from 100nm to 1 μm.

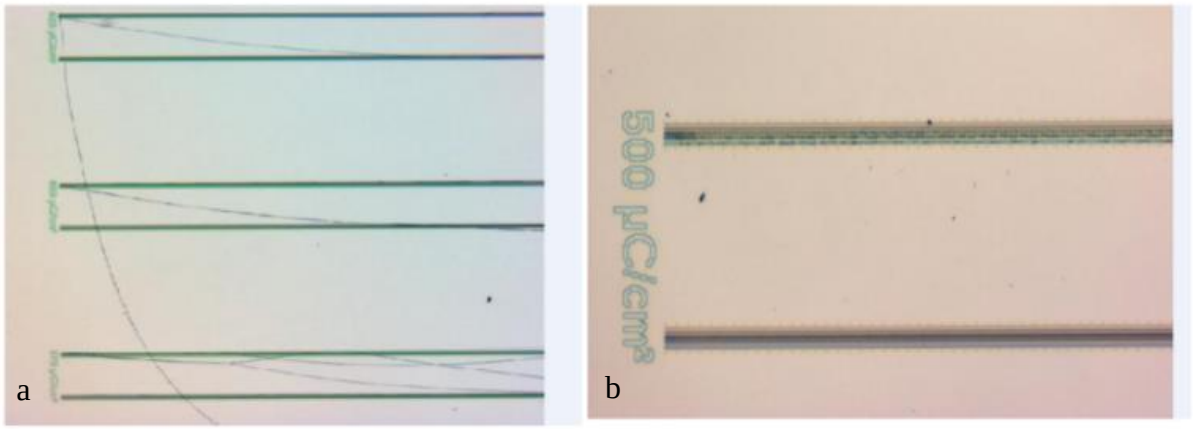

Figure 4.3 Optical images at different does of electron beam lithography. a) bridges are produced but they are collapsed. b) bridges are not formed in lower dose.

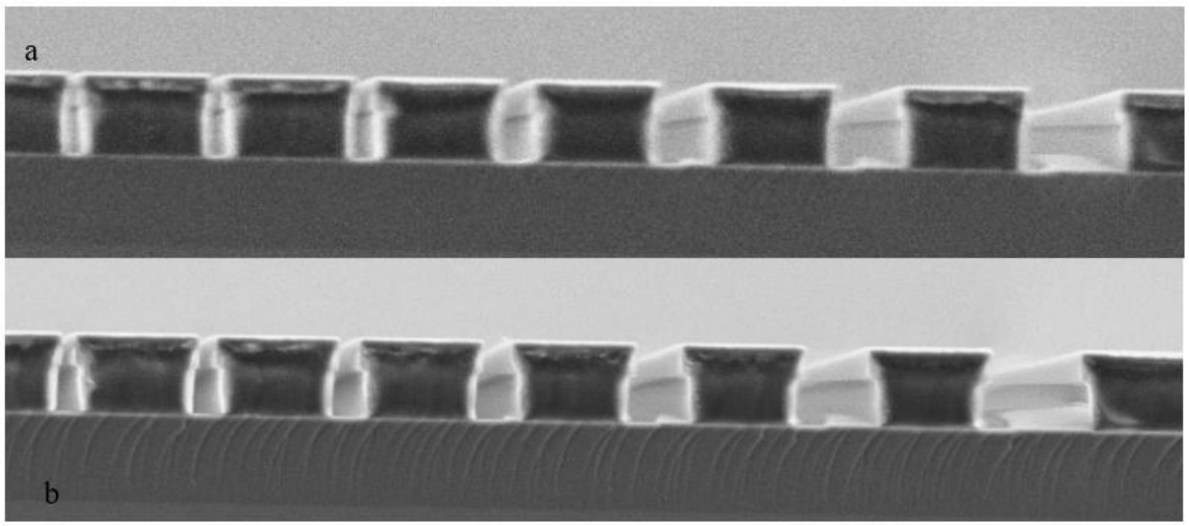

Figure 4.4 comparing the effect of dose on the undercut. Increasing the dose increases the undercut. a) SEM image of the sample at 700 µC/cm2, b) same sample with 1150 µC/cm2.

4.2.2 **Proximity effect correction (PEC)**

It is possible to produce a high-resolution pattern with Electron beam lithography, however, backscattering of electrons from the substrate leads to broadening of the exposed area which is called proximity effect. Proximity effect correction (PEC) is a method to reduce this effect which basically works by modifying the dose at certain areas Figure 4.5 shows the SEM images of similar patterns with the same dose developed by the same development process. The only difference is using the PEC.

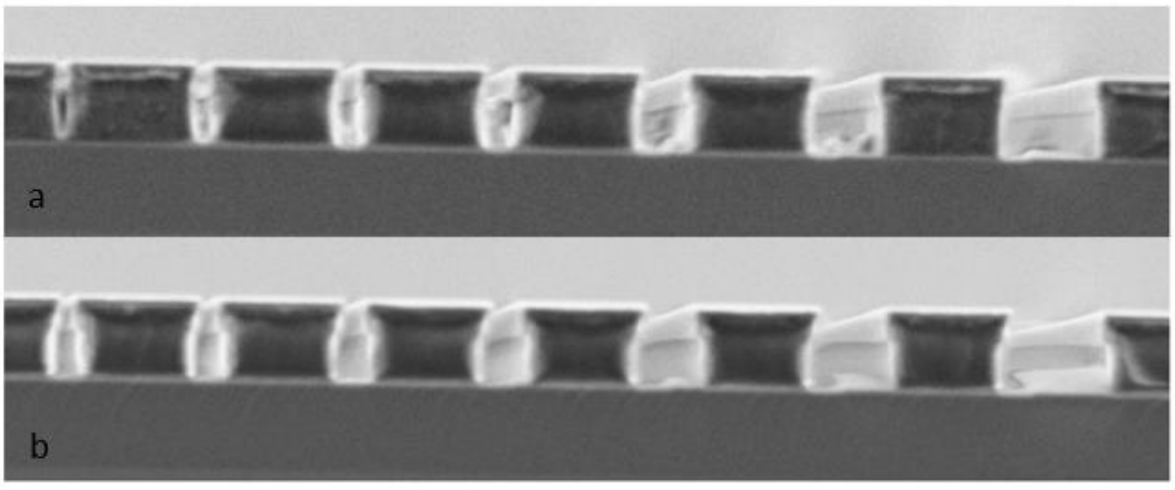

Figure 4.5 Proximity effect correction (PEC). a) without proximity effect correction. b) proximity effect correction results in better lithography process specifically for small features.

We finally used 1500 μC/cm^2 for pattering the Josephson junctions with proximity effect correction.

4.2.3 Development process

Development process also affect the undercut provided in the bi-layer resist system. We did series of optimization to achieve a reliable development recipe. Our standard development of PMMA is immersing the sample in mixture of MIBK (1): IPA (3) for 60 seconds and then rinsing it in IPA for 30 seconds, however, this does not lead to sufficient undercut for fabrication of the Josephson junctions. One factor that can increase the undercut during the development is time of the process. We increased the duration for MIBK (1): IPA (3) to 120 seconds. Figure 4.6 shows the development of patterns at different development time.

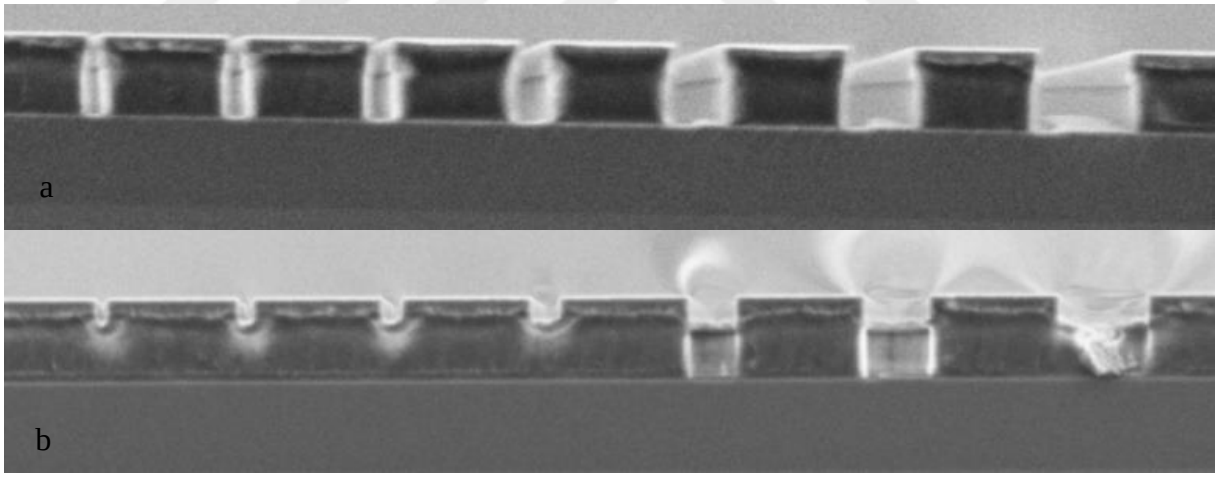

Figure 4.6 The effect of development time. Both samples are patterned with same dose and developed with a same procedure. a) development for 120seconds. b) development for 60 seconds.

So far, we realized doubling the development time of conventional development process increases the undercut, however, we still need a larger undercut for fabrication of Junctions. We added a strong solvent (Ethanol) to the process which remove larger volume of undercut from the resist[26]. Finally, the optimized process is achieved by changing the ratio of the mixing of the chemicals. The final recipe is as following:

1. Immersing the sample in 1: 2 mixtures of MIBK: IPA for 60 seconds.
2. Immersing the sample in 1: 2 mixtures of MIBK: IPA for 60 seconds.
3. Rinsing the sample in IPA for 30 seconds.

In each step, after removing the sample from solvent it is immediately put into the next solvent. At the end of the process, samples are blown with nitrogen.

4.3 Evaporation and Oxidation

After producing the desired pattern on the double layer resist substrate with EBL and developing it with the development method that ensures the efficiency of the undercut, it is time to deposit Al films. The sample is glued on the sample holder by Kapton tape and then installed inside the chamber. Tungsten basket is used for the evaporation of Al pellets. The general procedure for fabrication is evaporating 50 nm of Al at angle 15° and then oxidize the first layer for some certain amount of time and then evaporate 40 nm of Al at -15°.

The oxidation pressure and time affect the quality of the junction because they determine the thickness of the AlO_x barrier. Increasing the oxidation pressure and oxidation time yields to a thicker barrier that basically decreases the tunneling current across the Junction. Oxidation process is crucial part in fabrication of Josephson junction and one factor that highly defines the quality of the oxidation is roughness of first Al layer. Low quality deposition of Al results in pinholes or uneven barrier thickness on the oxide layer which both can prevent from a homogeneous oxide barrier. One way to make sure that deposited Al is smooth enough is to control the evaporation rate.

Heating problem

The distance between the source of evaporation and the sample should be long enough to prevent heating the sample because it can cause two major problems during fabrication process: first, heating may give rise to melting the resist; second, heating can break the oxide barrier which results in shorting the circuits.

For our homemade evaporation system, this distance is relatively short (Figure 2.1), and we observed similar problems during this work. Figure 4.7 indicates that second layer of

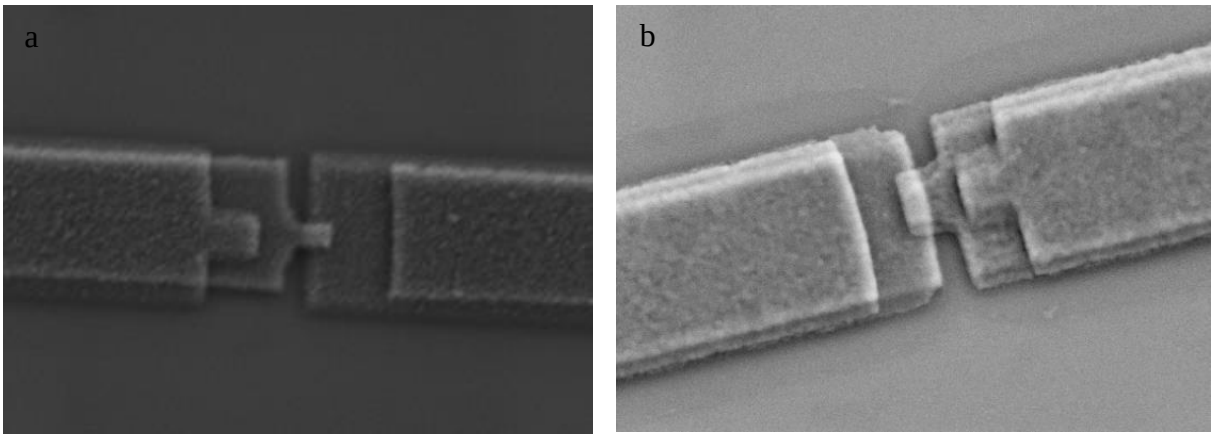

Figure 4.7 SEM image of Josephson junction fabricated in this work. a) the nose shape becomes smaller in second evaporation because of too much heating of the sample. b) the problem is solved after modifying the process by utilizing different tungsten boat in each round of evaporation.

evaporation becomes narrower which is due to melting of the resist and collapsing on substrate, this leads to narrowing of the openings, thus, narrowing of the second layer of Al.

The heating problem mostly happens during the second evaporation round due to depletion of the tungsten basket from Al pellet. Therefore, one solution to this problem is to use different sources for each round of evaporation to prevent the depletion of aluminum. Since our evaporation system is equipped with three thermal evaporation sources, we managed the heating problem by using two different sources instead of only one.

4.4 **Lift- off**

To get rid of the spare Al films and resist layers, we do the lift-off after evaporation process. This step is done by immersing the sample in hot Acetone(60°C) for 10 minutes. After that, we wait overnight to get cleaner lift-off however it is not compulsory. In this stage we expect that excess Al with resist get peeled off.

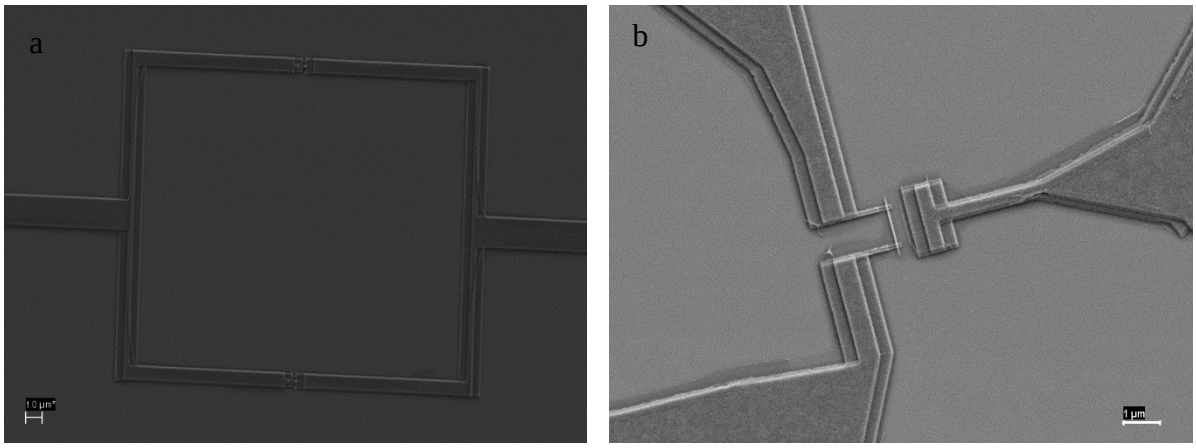

Figure 4.8 SEM image of samples fabricated during this work after lift-off process. a): DC-SQUID. b): single electron transistor

4.5 **Wire Bonding**

Wire bonding is a method typically used to connect the pins on the chip career to the wiring pads of the device. After dicing the samples to smaller dimensions, we glued the samples on the surface of the chip career with PMMA and baking for few minutes on the baker at 170°C. Gold wires are used to make the electrical contacts between the devices and the chip career pins with ball bonding method. In this method, gold wire is bonded to wiring pads of the device with ultrasonic vibration. Figure 4.9.a shows the TPT /HB16 Ball and Wedge Wire Bonder at SUNUM.

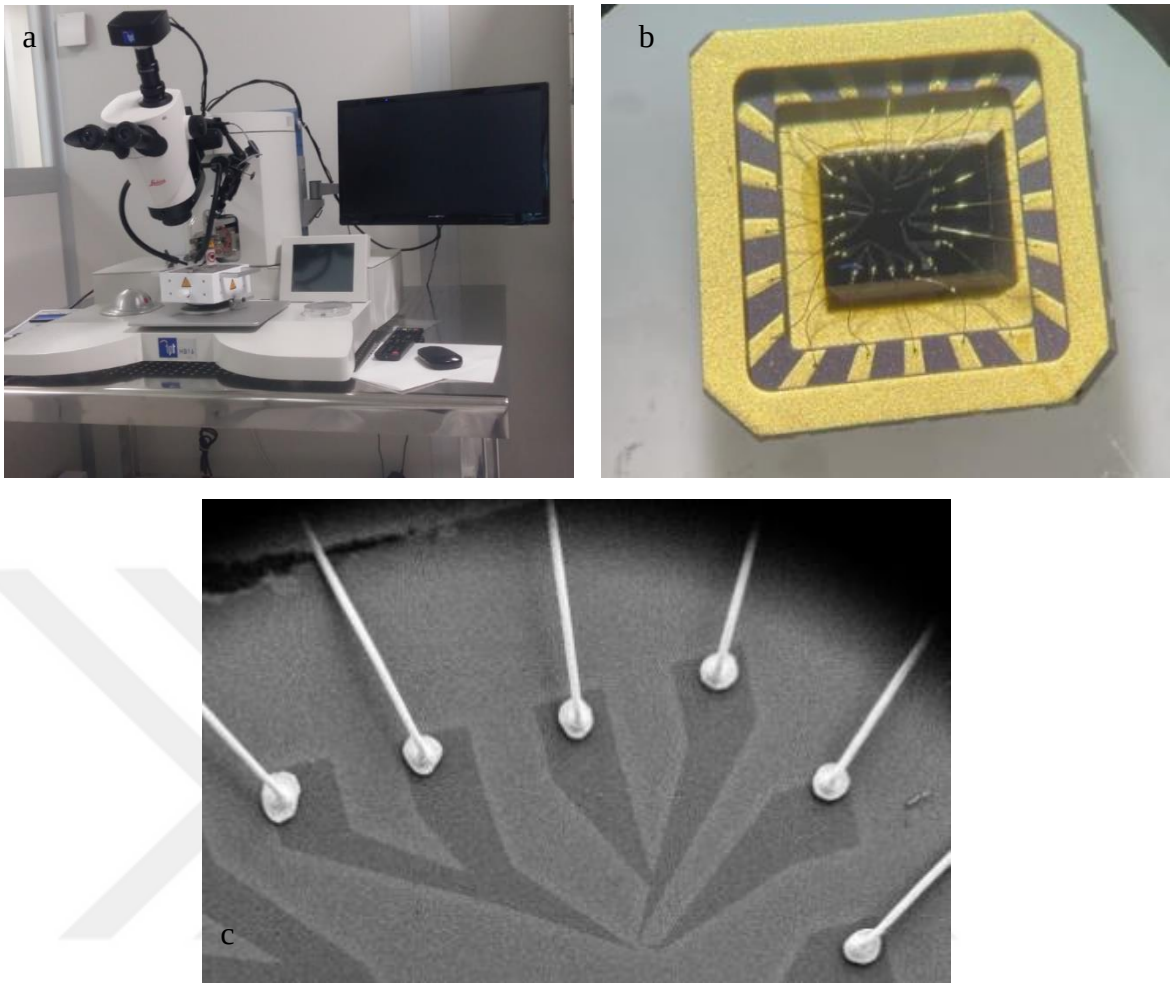

Figure 4.9 a) Photograph of TPT/HB16 wire bonder at SUNUM. b) photograph of a sample wire bonded with gold wires. c)SEM image of gold wire bonded on wiring pads of the device. The dimension of wiring pad is 200x200μm.

4.6 **Low temperature characterization**

The critical temperature of aluminum is 1.2K. This means for measuring superconducting quantum devices made from Al/AlO_x/Al Josephson junctions can be done only at temperature lower than 1.2K. Therefore, Oxford Triton 400 He^3/He^4 10mK dilution refrigerator (Figure 4.10) is used for the characterization of the devices.

Figure 4.10 a) Oxford triton 400 dilution refrigerator with electronic measurement setup and control unit. b) photograph of sample puck

4.6.1 Current-Voltage Characteristic

As described in sec.2.2.3, the I-V characteristic of Josephson junction shows non-linear behavior. At superconducting state there is not voltage develop across the junction and any current applied to the device can pass without any dissipation until it exceeds the critical current value. Then, it jumps to the normal state or voltage state where the behavior is almost linear.

For measuring the I-V characteristic of the devices, conventional 4-probe measurement is performed which ensures that any resistive element involved in the leads coming from cryostat is ignored. This works by applying current by a power source and reading out the voltage drop across the device by nanovoltmeter. The electrical instruments that we used during this work for quantum transport measurements are Agilent B2912A Source measurement Unit (SMU), Keysight B2962A Power Source Unit, and Keithley 22182A Nanovoltmeter.

Figure 4.11 shows I-V characteristic of device (RF-150821-sub1-1) which is a thin aluminum film fabricated during this work without shadow evaporation technique.

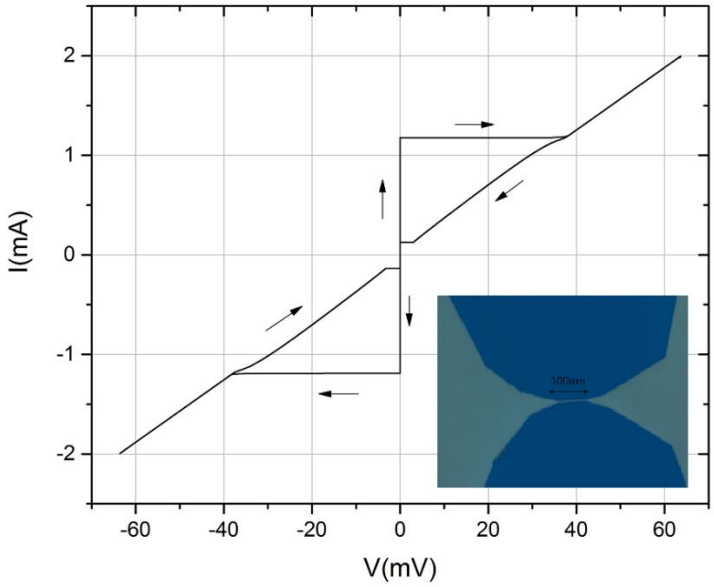

Figure 4.11 I-V characterization of thin film Al, fabricated without suspended bridge which means there is no junction overlap. The measurement is done with 4-probe technique (RF-150821-sub1-1).

As described in Sec.4.3 the thickness of the oxide barrier is dependent on the oxidation pressure and time. If the barrier becomes thick enough, we expect the junctions to behave as classical tunnel junctions where there is no cooper pair tunneling that means there is no superconducting state as it exists in the Josephson junctions. Figure 4.12 shows the I-V characteristic of a tunnel junction (device RF-250321-sub1-1) where there is only single electron tunneling across the junction. The tunneling effect vanishes at 30 mT which is higher than the critical magnetic field of the aluminum given in the literature(10 mT).

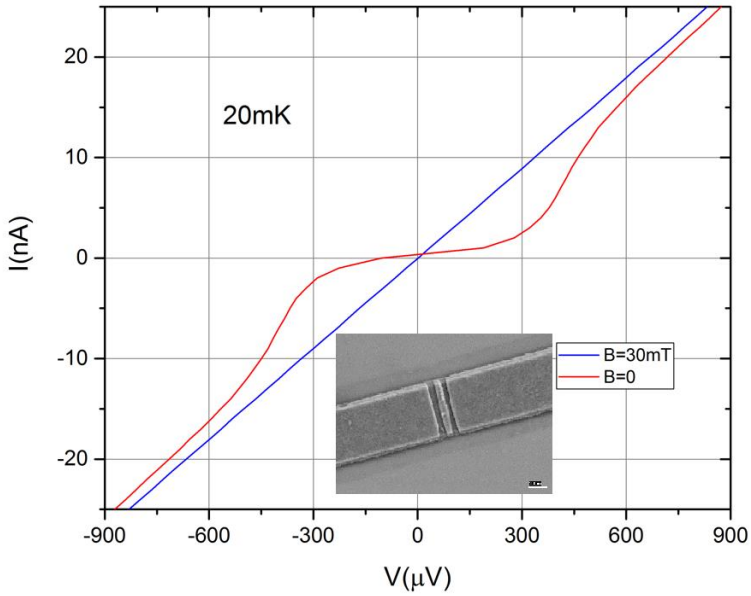

Figure 4.12 I-V characteristic of a classical SIS tunnel junction. There is no cooper pair tunneling and only single electrons tunnel through the junction (RF-250321-sub1-1).

Low temperature properties of p-type silicon

Josephson junctions are highly sensitive to electrostatic discharge, and they can easily get burned during the handling of the devices. Therefore, one way to prevent samples from electrostatic discharge is using silicon substrate which are conductive at room temperature. Figure 4.13 shows the I-V measurement of the silicon substrate at different temperatures, and Figure 4.14 shows the conductivity of silicon versus temperature. The conductance decreases exponentially by cooling down the device from 90 K to 10 K.

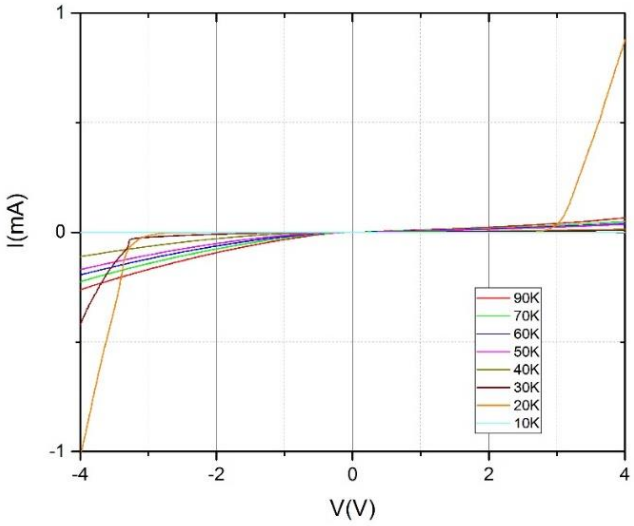

Figure 4.13 I-V plot of silicon substrate from 90 K down to 10 K. the conductance of silicon at 10K is zero.

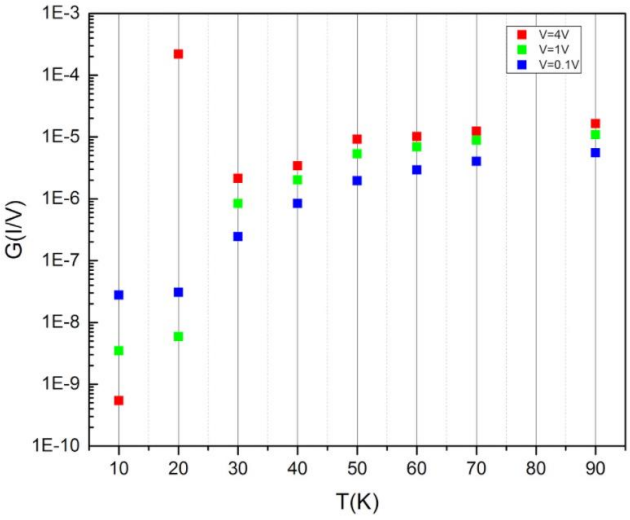

Figure 4.14 Electrical conductance vs. temperature of silicon in logarithmic scale for voltage values 0.1,1 and 4 V.

Observation of Josephson effect in a superconducting weak link

Josephson effect is a phenomenon that does not only occurs in tunnel junctions, it can also be clearly observed in the so called superconducting weak link[27] which was first observed in famous Anderson and Rowel experiment[28]. The critical current in short weak link is rather high, and their advantage over tunnel junction is small capacitance. Figure 4.15 shows the I-V plot of a device that has critical current density of 40KA/cm^2. This critical current density is higher than what we expect for a Josephson junction.

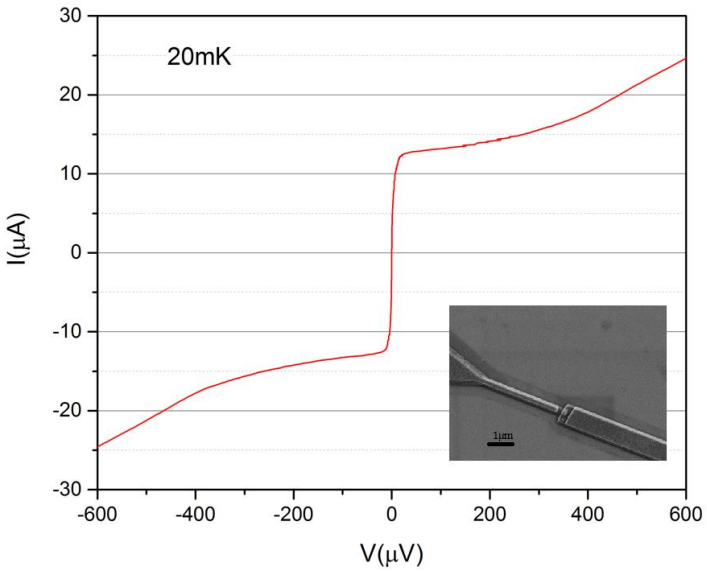

Figure 4.15 Josephson effect in superconducting weak link. Critical current is 15μA which is high for a typical Al/AlOx/Al Josephson junction. The voltage gap is roughly 300μV which agrees with Ambegaokar-Baratoff relation (sec 2.2.3). SEM image of similar device is shown. (RF-171220-sub2-1)

The I-V characterization (Figure 4.15) shows a high damping circuit where the capacitance of the circuit is extremely small. This low capacitance along with low resistance yields to vanishing β_c(Sec2.2.5).

Figure 4.16 shows I-V characterization of device (RF-171220-sub1-2) consisting of f two Josephson junctions in parallel. Comparing this with Figure 4.15, it can be understood that the critical current of RF-171220-sub1-1 is almost double as RF-171220-sub2-1. This is expected because the dimensions of the junctions in both devices are almost the same and they are from same fabrication round. However, RF-171220-sub1-2 does not react to small magnetic field applied on it unless the magnetic field reaches to the critical magnetic field of aluminum(10mT). This is another evidence for RF-171220-sub2-1 and RF-171220-sub1-2 are not being Josephson junctions, but are so called superconducting weak links.

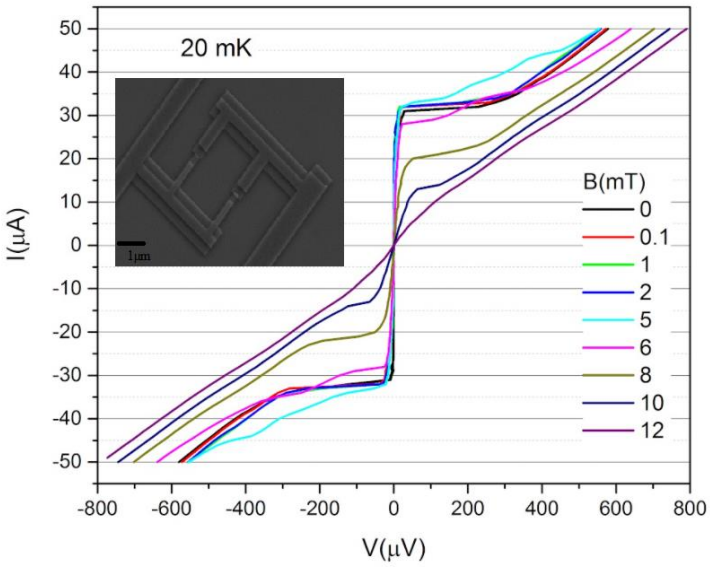

Figure 4.16 superconducting weak link in DC-SQUID configuration. The device does not respond to low external magnetic field. Near the critical magnetic field of aluminum, superconductivity starts vanishing. (RF-171220-sub1-2)

Josephson effect in DC-SQUID

As describe in Sec.2.3, DC-SQUID is a device consisting of two Josephson junctions in parallel. The critical current of DC-SQUID is 2*Ic*, where I_c is a critical current of single junction assuming both junctions are identical. The I-V characterization of DC-SQUID is similar to a single junction. Figure 4.17 shows the I-V measurement of DC-SQUID (sample RF-260521-sub2-4) including two Josephson junctions with dimensions approximately 200x300nm in 2x1μm superconducting loop.

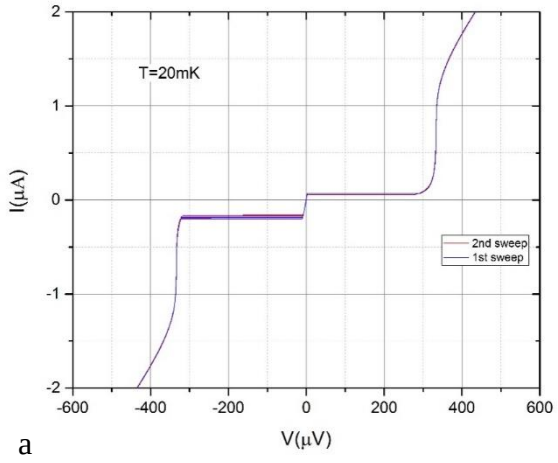

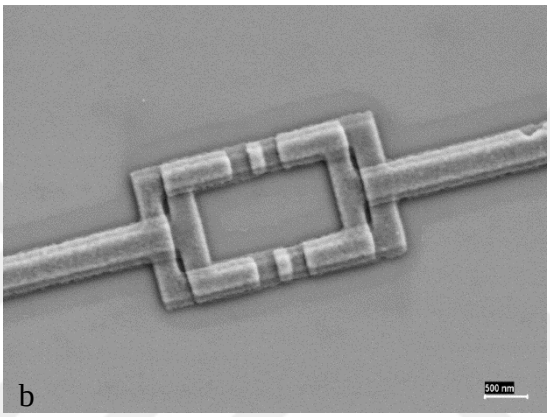

Figure 4.17 DC-SQUID. a) I-V characteristic of a DC-SQUID at zero magnetic field. The sample has very small hysteresis. b) SEM micrograph of a similar device (RF-260521-sub2-4).

The normal resistance of the device is $R_n \approx 215\ \Omega$ that can be estimated from Figure 4.17.a by considering the ohmic relations between current and voltage at the volage state ($V_c = I_c R$). When the normal resistance is low, we expect the circuit to have high critical current while this circuit shows a low critical current. This reason can be traced to the environmental noise which suppresses the superconducting current of the junctions. The actual critical current can be estimated from the I-V plot as 1.3μA which is the current that circuit switches to normal state.

The characteristic voltage of the circuits is 330 μV which is higher than what we expect in theory (Eq.1.9), one explanation for that is that aluminum gets incorporated with other atoms such as oxygen during evaporation, hence, the voltage gap of deposited aluminum increases which results into higher voltage state for the circuit.

Summary and outlook

Our main task in this thesis is optimizing performance factors for fabrication of sub-micron Josephson junction. This is very important since the parameters at different laboratories are quite different, and we managed to address the issues that we faced during this work to find a recipe for fabrication process.

We first studied the physics of Josephson junctions starting from historical background of superconductivity and introducing the Josephson equation to understand the non-linearity of Junctions. We then investigated DC-SQUID and demonstrated how external flux influence the critical current of the device. The rest of the theoretical study is dedicated to superconducting qubits and the reason why Josephson junctions has an important role in them.

First, we found a resist combination that yields to a proper undercut for shadow evaporation technique. As next step, we investigated the required dose for EBL process for patterning the samples on the double layer resist, then we obtained the sufficient undercut by optimizing the development procedure by studying the effect of development time, development ratio, and proper solvents for the process.

For the thermal evaporation, finding an appropriate evaporation source was crucial. We find that one critical problem in our evaporation process is the increasing of temperature inside the chamber. We tested different sources including tungsten boat, tungsten basket, and alumina thermal crucible and it turns out that by using tungsten basket, heating of the chamber is not too problematic comparing with the two other sources based on our evaporation system. Heating problem can lead to two major problems: melting the resist and leading to poor oxidation process because it affects the quality of deposited Al. The other factor that potentially influence the quality of Al thin film is the rate of the evaporation. For instance, an unstable rate gives rise to non-smooth layer, thus ending in poor oxidation. Therefore, by solving the heating problem and maintaining a stable evaporation rate we succeeded to fabricate junctions with well-stablished AlO_x barrier.

Electrostatic discharge (EDS) is a big challenge for characterization of Josephson junction since they are extremely sensitive to EDS. Our first attempt to solve this problem was to use silicon substrate instead of silicon oxide to take advantage of conductivity of

silicon at room temperature. Also, by fabrication multi junction circuits like DC-SQUID we observed that they are more resistance to EDS.

To cool down the samples below 1.2K, we used a dilution refrigerator where the sample is protected from environmental noise. We measured the I-V characterization of the devices with 4-probe measurement technique which is a common technique to ensure that the any resistive element expect the sample is ignored.

For the future of this work, we plan to investigate the effect of pressure and time of oxidation process on the quality of the junctions. Furthermore, we need to install filters inside our dilution refrigerator because we find the internal noise one influencing factor on the characterization of fabricated junctions.

Bibliography

1. Introduction to Superconductivity: Second Edition (Dover Books on Physics): Michael Tinkham

2. Nakamura, Y., Pashkin, Y. A. & Tsai, J. S. Coherent control of macroscopic quantum states in a single-Cooper-pair box. *Nature* **398**, 786–788 (1999).

3. Orlando, T. P. *et al.* A Superconducting Persistent Current Qubit. *Phys. Rev. B* **60**, 15398–15413 (1999).

4. Vion, D. *et al.* Manipulating the Quantum State of an Electrical Circuit. *Science* **296**, 886–889 (2002).

5. Koch, J. *et al.* Charge-insensitive qubit design derived from the Cooper pair box. *Phys. Rev. A* **76**, 042319 (2007).

6. Martinis, J. M., Nam, S., Aumentado, J. & Urbina, C. Rabi Oscillations in a Large Josephson-Junction Qubit. *Phys. Rev. Lett.* **89**, 117901 (2002).

7. Forrest, A. M. Meissner and Ochsenfeld revisited. *Eur. J. Phys.* **4**, 117–120 (1983).

8. London, F., London, H. & Lindemann, F. A. The electromagnetic equations of the supraconductor. *Proc. R. Soc. Lond. Ser. - Math. Phys. Sci.* **149**, 71–88 (1935).

9. Bardeen, J., Cooper, L. N. & Schrieffer, J. R. Theory of Superconductivity. *Phys. Rev.* **108**, 1175–1204 (1957).

10. Josephson, B. D. Possible new effects in superconductive tunnelling. *Phys. Lett.* **1**, 251–253 (1962).

11. Giaever, I. Energy Gap in Superconductors Measured by Electron Tunneling. *Phys. Rev. Lett.* **5**, 147–148 (1960).

12. Ambegaokar, V. & Baratoff, A. Tunneling Between Superconductors. *Phys. Rev. Lett.* **10**, 486–489 (1963).

13. Kiviranta, M. & Seppä, H. Effect of Voltage Bias on the dc SQUID Characteristics. *J. Low Temp. Phys.* **123**, 127–136 (2001).

14. Clarke, J. & Braginski, A. I. *The SQUID Handbook: Fundamentals and Technology of SQUIDs and SQUID Systems*. (Wiley-VCH, 2004).

15. DiVincenzo, D. P. The Physical Implementation of Quantum Computation. *Fortschritte Phys.* **48**, 771–783 (2000).

16. Vandersypen, L. M. *et al.* Experimental realization of Shor's quantum factoring algorithm using nuclear magnetic resonance. *Nature* **414**, 883–887 (2001).

17. Cirac, J. I. & Zoller, P. Quantum Computations with Cold Trapped Ions. *Phys. Rev. Lett.* **74**, 4091–4094 (1995).

18. Loss, D. & DiVincenzo, D. P. Quantum computation with quantum dots. *Phys. Rev. A* **57**, 120–126 (1998).

19. Houck, A. A. *et al.* Controlling the Spontaneous Emission of a Superconducting Transmon Qubit. *Phys. Rev. Lett.* **101**, 080502 (2008).

20. Sakurai, J. J. & Napolitano, J. *Modern quantum mechanics*. (Addison-Wesley, 2011).

21. Meyerhofer, D. Characteristics of resist films produced by spinning. *J. Appl. Phys.* **49**, 3993–3997 (1978).

22. Spin Coat Processing Theory. *Brewer Science* https://www.brewerscience.com/processing-theories/spin-coat/.

23. Dolan, G. J. Offset masks for lift-off photoprocessing. *Appl. Phys. Lett.* **31**, 337–339 (1977).

24. Wu, Y.-L. *et al.* Fabrication of Al/AlOx/Al Josephson junctions and superconducting quantum circuits by shadow evaporation and a dynamic oxidation process. *Chin. Phys. B* **22**, 060309 (2013).

25. Resistive Thermal Evaporation. *Angstrom Engineering* https://angstromengineering.com/tech/resistive-thermal-evaporation/.

26. Pop, I. M. *et al.* Fabrication of stable and reproducible submicron tunnel junctions. *J. Vac. Sci. Technol. B Nanotechnol. Microelectron. Mater. Process. Meas. Phenom.* **30**, 010607 (2012).

27. Likharev, K. K. Superconducting weak links. *Rev. Mod. Phys.* **51**, 101–159 (1979).

28. Anderson, P. W. & Rowell, J. M. Probable Observation of the Josephson Superconducting Tunneling Effect. *Phys. Rev. Lett.* **10**, 230–232 (1963).